Draft version October 22, 2019
Typeset using LaTeX **twocolumn** style in AASTeX62

arXiv:1910.09038v1 [astro-ph.SR] 20 Oct 2019

Testing the Spectroscopic Extraction of Suppression of Convective Blueshift

M. Miklos,[1,2] T. W. Milbourne,[1,2] R. D. Haywood,[2,*] D. F. Phillips,[2] S. H. Saar,[2] N. Meunier,[3] H. M. Cegla,[4,5,†] X. Dumusque,[4] N. Langellier,[1,2] J. Maldonado,[6] L. Malavolta,[7,8] A. Mortier,[9] S. Thompson,[10] C. A. Watson,[5] M. Cecconi,[11] R. Cosentino,[11] A. Ghedina,[11] C-H. Li,[2] M. López-Morales,[2] E. Molinari,[11,12] Ennio Poretti,[11,13,14] D. Sasselov,[2] A. Sozzetti,[15] and R. L. Walsworth[1,2]

[1] *Department of Physics, Harvard University, 17 Oxford Street, Cambridge MA 02138, USA*
[2] *Harvard-Smithsonian Center for Astrophysics, Cambridge, MA 02138, USA*
[3] *Univ. Grenoble Alpes, CNRS, IPAG, 38000 Grenoble, France*
[4] *Observatoire de Genève, Université de Genève, 51 chemin des Maillettes, 1290 Versoix, Switzerland*
[5] *Astrophysics Research Centre, School of Mathematics and Physics, Queen's University Belfast, Belfast BT7 1NN, UK*
[6] *INAF-Osservatorio Astronomico di Palermo, Piazza del Parlamento 1, 90134 Palermo, Italy*
[7] *INAF-Osservatorio Astronomico di Padova, Vicolo dell'Osservatorio 5, 35122 Padova, Italy*
[8] *Dipartimento di Fisica e Astronomia "Galileo Galilei", Università di Padova, Vicolo dell'Osservatorio 3, I-35122 Padova, Italy*
[9] *Astrophysics Group, Cavendish Laboratory, University of Cambridge, J.J. Thomson Avenue, Cambridge CB3 0HE, UK*
[10] *Astrophysics Group, Cavendish Laboratory, University of Cambridge, J.J. Thomson Avenue, Cambridge CB 0HE, UK*
[11] *INAF-Fundacion Galileo Galilei, Rambla Jose Ana Fernandez Perez 7, E-38712 Brena Baja, Spain*
[12] *INAF-Osservatorio Astronomico di Cagliari, Via della Scienza 5-09047 Selargius CA, Italy*
[13] *INAF-Osservatorio Astronomico di Brera, Via E. Bianchi 46, 23807 Merate (LC), Italy*
[14] *Centre for Exoplanet Science, University of Edinburgh, Edinburgh, UK*
[15] *INAF-Osservatorio Astrofisico di Torino, via Osservatorio 20, 10025 Pino Torinese, Italy*

ABSTRACT

Efforts to detect low-mass exoplanets using stellar radial velocities (RVs) are currently limited by magnetic photospheric activity. Suppression of convective blueshift is the dominant magnetic contribution to RV variability in low-activity Sun-like stars. Due to plasma motion driven by convective processes, the magnitude of RV contributions from the suppression of convective blueshift is proportional to the depth of formation of photospheric spectral lines used to compute the RV time series. Meunier et al. 2017 used this relation to demonstrate a method for spectroscopic extraction of the suppression of convective blueshift in order to isolate RV contributions, including planetary RVs, that contribute equally to the timeseries for each spectral line. Here, we extract disk-integrated solar RVs from observations over a 2.5 year time span made with the solar telescope integrated with the HARPS-N spectrograph at the Telescopio Nazionale Galileo (La Palma, Canary Islands, Spain). We apply the methods outlined by Meunier et al. 2017. We are not, however, able to isolate physically meaningful contributions of the suppression of convective blueshift from this solar dataset, potentially because our dataset is from solar minimum when the suppression of convective blueshift may not sufficiently dominate activity contributions to RVs. This result indicates that, for low-activity Sun-like stars, one must include additional RV contributions from activity sources not considered in the Meunier et al. 2017 model at different timescales as well as instrumental variation in order to reach the sub-meter per second RV sensitivity necessary to detect low-mass planets in orbit around Sun-like stars.

Keywords: techniques: radial velocities — Sun: activity — Sun: faculae, plage — Sun: granulation — sunspots — planets and satellites: detection

1. INTRODUCTION

The radial velocity (RV) method is the principal technique for constraining the masses of exoplanets (Mayor & Queloz 1995). It provides complementary information to the transit method, e.g., as used by the *Kepler* and TESS spacecraft (Borucki et al. 2010; Howell et al. 2014; Ricker et al. 2014) and ground-based transit surveys.

* NASA Sagan Fellow
† CHEOPS Fellow, SNSF NCCR-PlanetS

The Keplerian reflex motion induced in a Sun-like star by an Earth-mass planet in the habitable zone is of order 10 cm s^{-1} (Fischer et al. 2016), the target sensitivity of next-generation spectrographs (Pepe et al. 2010). However, contributions to observed stellar RVs from photospheric stellar activity often exceed 1 m s^{-1} even in the quietest Sun-like stars, posing a significant barrier to the detection of exoplanets by the RV method (e.g. Saar & Donahue 1997; Schrijver & Zwaan 2000; Isaacson & Fischer 2010; Motalebi et al. 2015). Several recent works describe a variety of models to mitigate the effects of magnetic activity on stellar RVs. One approach has been to study the Sun as a star, extracting solar activity estimates from images of the solar surface (Meunier et al. 2010a; Haywood et al. 2016; Milbourne et al. 2019) and comparing to simultaneous disk-integrated spectral measurements. In order to reduce unwanted stellar signals from exoplanet searches, however, methods for extracting stellar activity directly from spectra, and not from ancillary datasets, must be developed.

For Sun-like stars with low activity, suppression of convective blueshift due to photospheric plage (hereafter $\mathrm{RV_{conv}}$) dominates over the wavelength-independent photometric effects due to spots, or RV shifts induced by Earth-like exoplanets (Meunier et al. 2010b; Dumusque et al. 2014; Haywood et al. 2016) (hereafter $\mathrm{RV_{sppl}}$). Meunier et al. (2017a) (hereafter M17) have developed one model to isolate $\mathrm{RV_{conv}}$ contributions based on the correlation between relative depths and absolute RV blueshifts of spectral lines driven by plasma flow in granules. Rising plasma low in the photosphere exhibits strong RV blueshift, while plasma closer to the surface has most of its motion directed tangentially as it merges into intergranular lanes, thus exhibiting less RV blueshift (Dravins et al. 1981). While many factors such as temperature, electron pressure, and atomic constants affect spectral line relative depth (Gray 2005), line depth shows strong anti-correlation with height of formation in the stellar photosphere. Therefore, absolute radial velocity blueshift shows a strong relationship with line depth, commonly referred to as the third signature of stellar granulation (Gray 2009; Reiners et al. 2016; Meunier et al. 2017b; Gray & Oostra 2018). M17 leverage the dominance of $\mathrm{RV_{conv}}$ to write the RV time series derived from a set of lines s_0 as

$$\mathrm{RV}_0 = \mathrm{RV_{sppl}} + \mathrm{RV_{conv}} \tag{1}$$

where RV_0 is the radial velocity measured with this specific line list. $\mathrm{RV_{conv}}$ are line-list dependent contributions due to the suppression of convective blueshift, and $\mathrm{RV_{sppl}}$ are photometric variations (e.g. spots and plage), planetary signals, or other RV sources that are the same for all spectral lines.

In this model, an RV time series from a sublist s_1 of s_0 with a restricted flux range can be written

$$\mathrm{RV}_1 = \mathrm{RV_{sppl}} + \alpha \mathrm{RV_{conv}} \tag{2}$$

where α is the ratio of the shift in radial velocity by suppression of convective blueshift from line list s_1 compared to line list s_0. Based on the third signature of granulation (Gray 2009), we would expect $\alpha < 1$ for a sublist s_1 comprising strong lines formed close to the top of the photosphere, and $\alpha > 1$ for a sublist of weak lines, formed deep in the photosphere. If a precise value for α is known or can be inferred, we can invert the observed RV_0 and RV_1 time series to extract time series of interest RV_{conv} and RV_{sppl}.

Using time series $\mathrm{RV_{conv}}$ and $\mathrm{RV_{sppl}}$ extracted from solar photospheric images, M17 construct synthetic time series RV_0 and RV_1 using a value for α fitted from a solar atlas (Kurucz et al. 1984; Kurucz 2005) and added white noise. The authors then test several methods for estimating α on these synthetic time series, finding good convergence for the value of α across the methods (within 5% of the true value for low-noise conditions) (M17). Using this calculated value of α, they then recover and validate the original $\mathrm{RV_{sppl}}$ time series. Ideally, this technique could be utilized to correct RV time series for $\mathrm{RV_{conv}}$ contributions to lower the RV activity threshold.

On real data, determining an absolute scale for radial velocities is challenging, making it difficult to precisely determine α. M17 apply these methods to HARPS exposures of HD207129 but find no agreement for values of α derived by different estimation methods, which they attribute to infrequent observations and low SNR.

Using the solar telescope (Phillips et al. 2016) operating with the HARPS-N spectrograph at the Telescopio Nazionale Galileo (TNG, Cosentino et al. 2012), we extract high-resolution disk-integrated solar spectra (Dumusque et al. 2015). We now have more than 50,000 high-SNR solar exposures spanning over 4 years of observing (Collier Cameron et al. 2019). In this work, we apply Meunier's methods to the first 2.5 years of the solar dataset (from Summer 2015 - November 2017) to attempt a recovery of a precise value of α for use in reconstructing $\mathrm{RV_{conv}}$ and $\mathrm{RV_{sppl}}$. In Section 2, we discuss our method for extracting line-by-line RVs from the HARPS-N solar spectra. In Section 3, we discuss various techniques for determining α from the resulting RV timeseries, and attempt to compute consistent α values. We conclude in Section 4 with a discussion of the result-

ing values, and possible explanations for why the model does not reduce RV RMS on our dataset

2. METHODS

2.1. *Extracting RVs from HARPS-N spectra*

Third signature plots in the literature are often based on neutral iron lines to demonstrate the relationship between relative depth and absolute convective blueshift (Gray 2009; Reiners et al. 2016; Gray & Oostra 2018). In order to compare lines known to exhibit the third signature effect, we consider a line list from the NIST database for Fe I lines[1]. We extract disk-integrated HARPS-N solar spectra over a 2.5 year span, with an average of 51 exposures per day. We cut data taken in overcast weather, as identified using the HARPS-N exposure meter, and reject data for any day with five or fewer exposures. Each spectrum is shifted to a heliocentric reference frame using relative velocities from the JPL Horizons ephemeris (Giorgini et al. 1996). We normalize the spectrum continuum by dividing by the corresponding blaze measurement - we propagate the photon shot noise error from each into the fits of each spectral line, as described below.

For each individual spectral line, we stack the Doppler-shifted measurements from a given day to produce a composite line profile for each day. This approach, stacking data from different exposures instead of averaging over multiple exposures, avoids interpolating data onto a common wavelength grid. We fit the line core (0.2 Angstroms total) with Gaussian profiles to extract relative depth, and line center (0.1 Angstroms total) with 2nd-degree polynomials to measure the RV. We adopted polynomial fits to best mirror the methods of M17. We then convert these line center positions from wavelength to RV. This process is illustrated in Figure 1. Removing poorly-fit and blended lines results in a final list of 765 spectral lines.[2]

The relative velocities derived reproduce the shape of the third signature curve from Reiners et al. (2016) up to an overall offset, as shown in Figure 2. This offset may result from differences between the line lists or instruments used.

2.2. *Zeroing RV time series*

It is challenging to extract absolute RVs from spectral data. In accounting for blueshifts of individual spectral lines, we must identify the hypothetical RV value achieved in the absence of stellar activity, which will vary from line to line, in a manner that is robust against outlier points or noise. We zero the radial velocity time series per spectral line to account for this absolute blueshift. We sort time series observations by RV value per line, and subtract the average of the middle two quartiles, as shown in Figure 1. In selecting this range, we assume that low-activity days will fall close to the median value; by subtracting the average value for the low-activity days, we aim to identify the hypothetical no-activity point for each line while avoiding bias in our zero point due to outliers.

Table 1. Features of RV time series extracted from HARPS-N/solar telescope daily binned spectra.

	RV_0	RV_1	RV_2
Relative Depth	.05-.95	.5-.95	.05-.5
Number of Lines	765	386	379
Standard Deviation (m s^{-1})	1.50	1.64	1.74
Mean (m s^{-1})	.47	.37	.59

2.3. *Finding RVs from sublists*

Following the procedure of M17, we identify line sublists by relative depth. We take variance-weighted means of the entire line list (s_0), lines with relative depth .5-.95 (s_1), and lines with relative depth .05-.5 (s_2), to extract RV_0, RV_1, and RV_2 respectively. The RV errors are computed from fit errorbars on the line center parameter, which incorporate propagated shot noise from the raw spectra. Features of these time series are listed in Table 1.

To validate our extracted time series, we compare to the HARPS-N Data Reduction System (DRS) RVs (Baranne et al. 1996; Sosnowska et al. 2012). Figure 3 shows a Lomb-Scargle periodogram comparison of the two time series (Zechmeister & Kürster 2009; VanderPlas et al. 2012; VanderPlas & Ivezić 2015). Many of the periods with highest concentration of signal power align between the two series, suggesting that they capture the same solar physics. We note that the power concentrated at rotation and half-rotation periods in RV_1 exceeds that of RV_2, normalizing to the false alarm probability (FAP). While the RMS scatter of RV_2 is greater than RV_1, we find that over 1.5 ms^{-1} of white noise would need to be added to RV_2 compared to RV_1 to account for this difference in peak heights. The model from M17 would predict, however, that since RV_2 is calculated from lines presumably formed lower in the stellar photosphere, it should be more dominated by the suppression of convective blueshift, which would imply that this trend should be reversed. This observation

[1] https://physics.nist.gov/PhysRefData/ASD/lines_form.html
[2] Full line list available online with supplemental material.

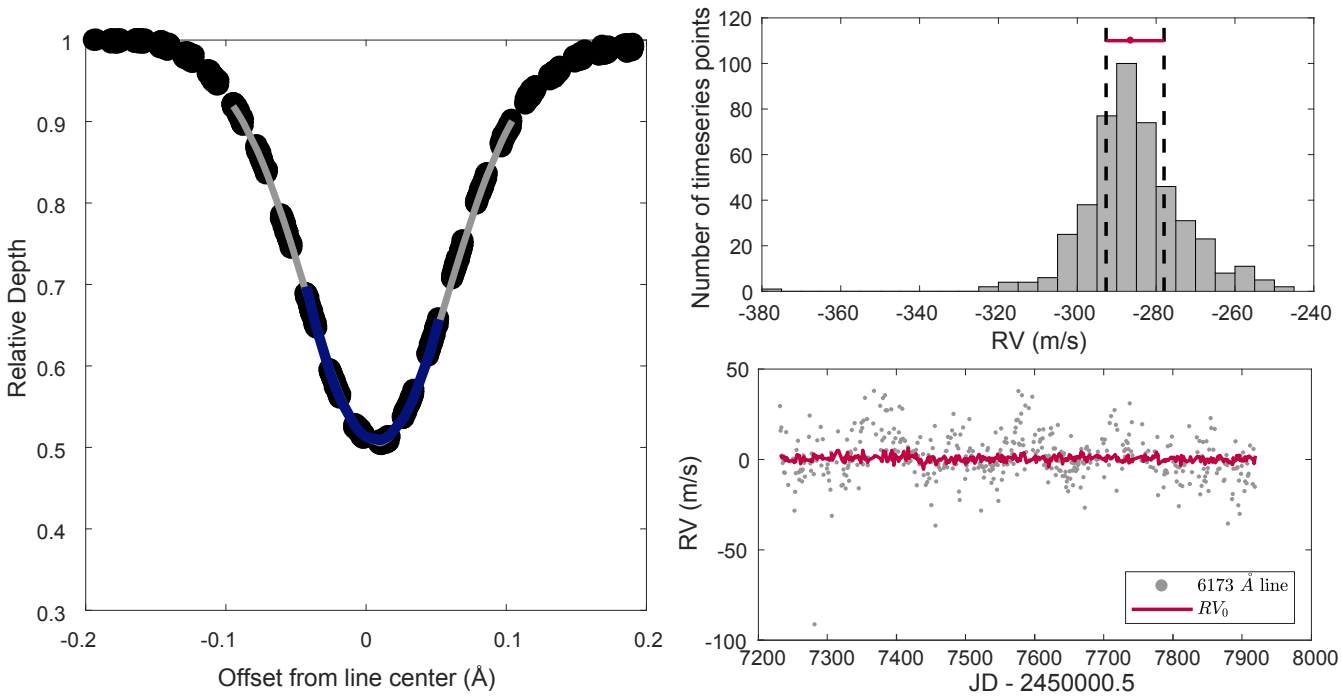


Figure 1. Left: Illustration of boundaries of observed points (black) included in fits for Gaussian (gray curve) and polynomial (dark blue curve) fits for a representative line (at 6173 Å). Right, top: demonstration of zeroing procedure for same 6173 Å line– the average of the middle two quartiles of RV values per line is subtracted off. Right, bottom: zeroed RV time series for 6173 Å line (gray), compared to average time series for all lines, RV_0 (red).

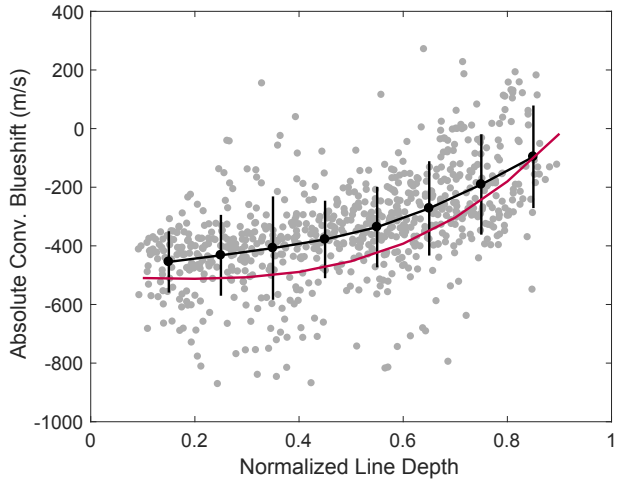


Figure 2. Third signature of stellar granulation trend demonstrated in Fe I list extracted from NIST database. Lines are binned in 0.1 relative depth bins: black dots show the average value per bin, and errorbars show standard deviation per bin. The red curve shows the polynomial of best fit from Reiners et al. (2016).

presents the first suggestion that one of the assumptions that underlies the model is not realized on this dataset.

3. ANALYSIS

3.1. *Solving for* α

If α is known, we can use experimentally determined values for RV_0 and RV_1 to extract theoretical time series of interest $\mathrm{RV}_{\mathrm{conv}}$ and $\mathrm{RV}_{\mathrm{sppl}}$. This process should isolate contributions from the suppression of convective blueshift, and leave behind common-mode planetary and photometric contributions in the corrected RV time series. In practice, however, we must estimate the parameter α by imposing assumptions on the reconstructed time series. We adopt methods to solve for the parameter α based on assumptions made for the reconstructed time series from M17. These methods rely predominantly on the assumption that $\mathrm{RV}_{\mathrm{conv}}$ dominates the RV time series. We applied the five methods detailed in M17 to solve numerically for the value of α that: 1) minimizes the mean absolute value of $\mathrm{RV}_{\mathrm{sppl}}$; 2) minimizes the correlation between $\mathrm{RV}_{\mathrm{conv}}$ and $\mathrm{RV}_{\mathrm{sppl}}$; 3) is the slope of RV_0 vs RV_1; 4) maximizes the ratio of the variance in $\mathrm{RV}_{\mathrm{conv}}$ vs that in $\mathrm{RV}_{\mathrm{sppl}}$; 5) maximizes that ratio when $\mathrm{RV}_{\mathrm{sppl}}$ is smoothed over 30 days, to average over rotationally modulated activity-induced variations. Additionally, 6) we calculate a best estimate for α as the ratio of the mean values of absolute RV time series derived from $\langle \mathrm{RV}_0 \rangle / \langle \mathrm{RV}_1 \rangle$ or $\langle \mathrm{RV}_0 \rangle / \langle \mathrm{RV}_2 \rangle$.

Table 2. Estimates for α, and RMS variation for extracted RV_{sppl} time series (m s^{-1}) from different methods. Method 2 fails to converge likely due to correlated noise, as discussed in M17

Method	RV_1, α	RV_1, std(RV_{sppl})	RV_2, α	RV_2, std(RV_{sppl})
1) $\langle RV_{sppl} \rangle = 0$	.79	3.54	1.26	3.60
2) Minimize correlation between RV_{sppl}, RV_{conv}	N/A	N/A	N/A	N/A
3) Slope of RV_0 vs RV_i	.97	22.63	1.03	28.54
4) Maximize std(RV_{conv})/std(RV_{sppl})	.99	67.79	1.01	85.56
5) Maximize std(RV_{conv})/std(RV_{sppl} smoothed 30 days)	.73	2.91	1.34	2.91
6) $\langle RV_{0,abs} \rangle / \langle RV_{i,abs} \rangle$	.74	2.99	1.32	3.05

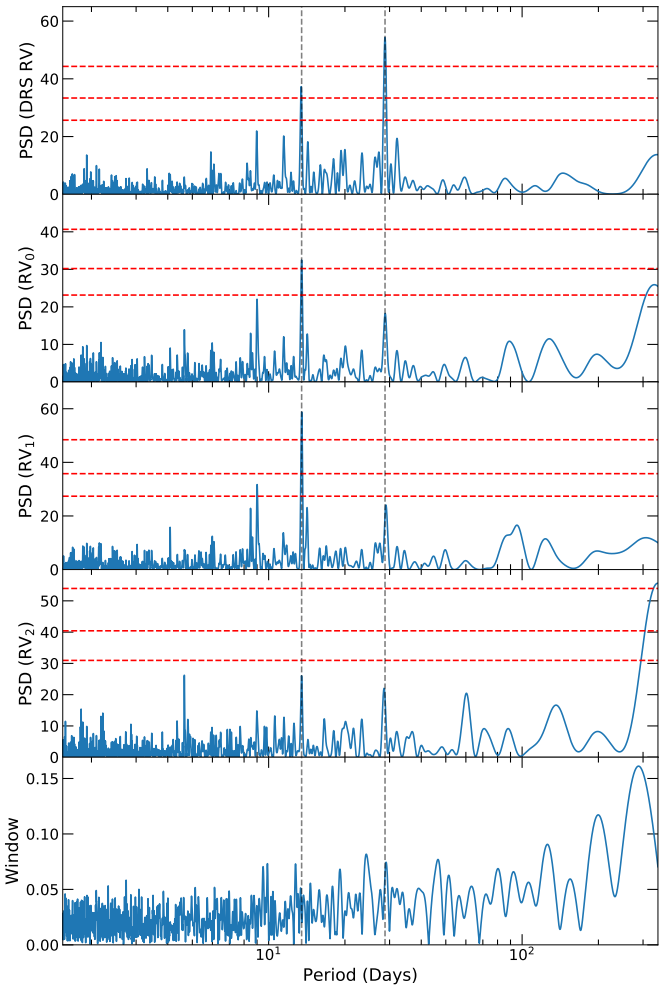


Figure 3. Lomb-Scargle periodograms of the DRS-reduced RVs, as well as the RV_0, RV_1, and RV_2 time series generated from our line lists. The 10%, 1%, and 0.1% False Alarm Probabilities (red dotted lines) are shown for each periodogram. The greatest power is concentrated in the solar synodic rotation period and its first harmonic (dotted gray lines), with no corresponding peaks in the window function (bottom panel).

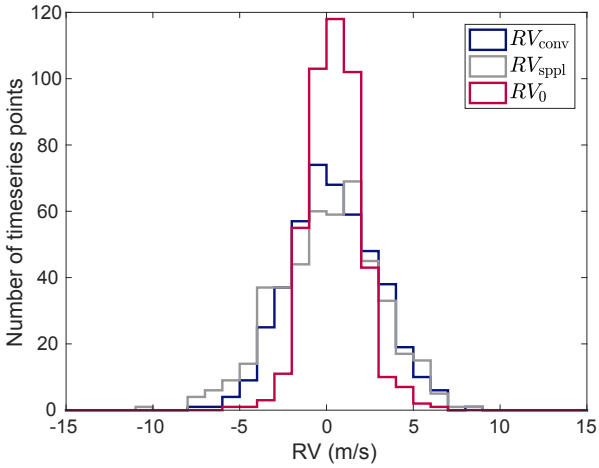


Figure 4. Histogram of timeseries points of RV_0, and treated timeseries RV_{sppl}, RV_{sppl} reconstructed using RV_1 for $\alpha = .73$: this reconstruction had the lowest RV RMS for RV_{sppl}. As shown, this reconstruction fails to reduce the RMS from the initial timeseries RV_0.

These values are shown in Table 2. Despite the relatively consistent observational sampling and high SNR of over 300 per exposure with an average of over 50 exposures per day, values for α differ based on the choice of assumption. Crucially, no physically motivated choice of α reduces the variability of RV_{sppl}, the corrected RV time series, compared to RV_0, the untreated time series, as illustrated in Figure 4.

4. DISCUSSION

Despite the higher SNR and better observational sampling for solar spectra, we are unable to extract physically significant reconstructed time series RV_{conv} and RV_{sppl} using the model and methods described in M17, suggesting that one of the assumptions of the model is not satisfied on this dataset. Crucially, the methods to estimate α assume that RV_{conv} strongly dominates the RV timeseries. Potentially important is that our data set spans the activity minimum of the solar cycle, unlike the synthetic dataset from M17, which included a full solar activity cycle: the assumption that RV_{conv} strongly

dominates the RV time series might not hold for these restricted observations. Since the process of inverting the linear equations that describe (RV_0, RV_1) to extract (RV_{sppl}, RV_{conv}) amplifies all non-RV_{conv} contributions, weakened RV_{conv} at solar minimum could explain the inability to extract physical values of α on this data set. Our inability to reduce RV variability by applying the methods of M17 implies that sources of RV variability other than RV_{conv} must be taken into account.

Additional results in the literature have shown that other processes besides RV_{conv} may indeed play a dominant role near the solar minimum. For example, recent techniques demonstrate the ability to remove most power at the rotation period, but leave 1 m s^{-1} RV variability in corrected timeseries: Dumusque (2018) and Cretingier et al. (2019, in revision) identify spectral lines insensitive to the suppression of convective blueshift; by computing RVs using these specially-selected line lists, the authors are able to reduce the RV RMS by a factor of 2.2, down to 0.9 m s^{-1}. Independently, Milbourne et al. (2019) use solar images from HMI/SDO to reproduce the activity-driven RVs. This analysis successfully removes the activity-driven signal at the rotation period, but still leaves an RMS amplitude of 1.2 m s^{-1}. Using independent analysis frameworks, both techniques successfully remove the rotationally-modulated activity signal, but are still limited by some other processes. Other work is ongoing to characterize the contributions from granulation and supergranulation, which can contribute as much as 1 m s^{-1} to RV RMS (Dumusque et al. 2011; Meunier et al. 2015; Meunier & Lagrange 2019; Cegla et al. 2019). The fact that our RV timeseries contain power concentrated at the rotation period and its harmonics is consistent with some significant RV_{conv} contribution.[3] The inability to significantly reduce RV RMS using the methods of M17 makes sense in the context of Milbourne et al. (2019), Dumusque (2018), the literature on granulation and supergranulation, which demonstrate that well over 1 m/s of RV variation remains after accounting for RV_{conv}.

When the linear equations defining RV_0 and RV_1 in terms of RV_{sppl} and RV_{conv} are inverted in the presence of noise introduced by this external variability, the RMS of noise in RV_{sppl} is magnified to twice as large as the original RMS of noise in RV_0 (M17). Potential contributions from instrumental systematics due to wavelength calibration (Cosentino et al. 2014; Dumusque 2018; Cersullo et al. 2019; Coffinet et al. 2019), or daily calibration sequences (Collier Cameron et al. 2019), may also contribute significantly to this non-RV_{conv} RV variability. This sensitivity to RV contributions other than RV_{conv} motivates future consideration of different solar activity processes, especially those operating on different timescales such as magnetoconvection (Palle et al. 1995; Del Moro 2004; Meunier 2018). Furthermore, these additional processes, and even the suppression of convective blueshift itself, may contain subtle line list dependency, based on proxies for line responsiveness to magnetic activity such as the Lande-g factor (e.g., Norton et al. 2006). All of these contributions must be accounted for in order to reach the 10 cm s^{-1} detection limit of an Earth-like planet orbiting a Sun-like star. Future work is needed to identify correlates in spectra, solar images, or some other ancillary dataset that could be used to model these phenomenon.

[3] We note, however, that concentration of high-activity regions separated by 180 degrees longitude on the Sun containing not only plage but also long-lived sunspots that contribute to RV_{sppl} through the photometric effect can also supply power at the rotation period (Schroeter 1984; Shelke & Verma 1985); similar structure exists on other Sun-like stars (Berdyugina & Järvinen 2005).

This work was supported in part by NASA award number NNX16AD42G and the Smithsonian Institution. Based on observations made with the Italian *Telescopio Nazionale Galileo* (TNG) operated by the *Fundación Galileo Galilei* (FGG) of the *Istituto Nazionale di Astrofisica* (INAF) at the *Observatorio del Roque de los Muchachos* (La Palma, Canary Islands, Spain). The solar telescope used in these observations was built and maintained with support from the Smithsonian Astrophysical Observatory, the Harvard Origins of Life Initiative, and the TNG.

This work was performed in part under contract with the California Institute of Technology (Caltech)/Jet Propulsion Laboratory (JPL) funded by NASA through the Sagan Fellowship Program executed by the NASA Exoplanet Science Institute (R.D.H.).

A.C.C. acknowledges support from STFC consolidated grant number ST/M001296/1.

D.W.L. acknowledges partial support from the *Kepler* mission under NASA Cooperative Agreement NNX13AB58A with the Smithsonian Astrophysical Observatory.

S.S. acknowledges support by NASA Heliophysics LWS grant NNX16AB79G.

H.M.C. acknowledges the financial support of the National Centre for Competence in Research PlanetS supported by the Swiss National Science Foundation (SNSF)

X. D. is grateful to the Branco-Weiss fellowship–Society in Science for continuous support.

This publication was made possible through the support of a grant from the John Templeton Foundation. The opinions expressed are those of the authors and do not necessarily reflect the views of the John Templeton Foundation.

This material is based upon work supported by the National Aeronautics and Space Administration under grants No. NNX15AC90G and NNX17AB59G issued through the Exoplanets Research Program. The research leading to these results has received funding from the European Union Seventh Framework Programme (FP7/2007-2013) under grant Agreement No. 313014 (ETAEARTH).

This work was supported in part by the NSF-REU solar physics program at SAO, grant number AGS-1560313.

The HARPS-N project has been funded by the Prodex Program of the Swiss Space Office (SSO), the Harvard University Origins of Life Initiative (HUOLI), the Scottish Universities Physics Alliance (SUPA), the University of Geneva, the Smithsonian Astrophysical Observatory (SAO), and the Italian National Astrophysical Institute (INAF), the University of St Andrews, Queen's University Belfast, and the University of Edinburgh.

This research has made use of NASA's Astrophysics Data System.

We thank the entire TNG staff for their continued support of the solar telescope project at HARPS-N.

Facility: TNG:HARPS-N

REFERENCES

Baranne, A., Queloz, D., Mayor, M., et al. 1996, A&AS, 119, 373

Berdyugina, S. V., & Järvinen, S. P. 2005, Astronomische Nachrichten, 326, 283

Borucki, W. J., Koch, D., Basri, G., et al. 2010, Science, 327, 977

Cegla, H. M., Watson, C. A., Shelyag, S., Mathioudakis, M., & Moutari, S. 2019, The Astrophysical Journal, 879, 55

Cersullo, F., Coffinet, A., Chazelas, B., Lovis, C., & Pepe, F. 2019, A&A, 624, A122

Coffinet, A., Lovis, C., Dumusque, X., & Pepe, F. 2019, A&A, 629, A27

Collier Cameron, A., Mortier, A., Phillips, D., et al. 2019, Monthly Notices of the Royal Astronomical Society, 487, 1082

Cosentino, R., Lovis, C., Pepe, F., et al. 2012, Proc.SPIE, 8446, 8446

—. 2014, Proc.SPIE, 9147, 9147

Cretingier, M., Dumusque, X., Allart, R., Pepe, F., & Lovis, C. 2019, in revision, A&A

Del Moro, D. 2004, A&A, 428, 1007

Dravins, D., Lindegren, L., & Nordlund, A. 1981, A&A, 96, 345

Dumusque, X. 2018, A&A, 620, A47

Dumusque, X., Boisse, I., & Santos, N. C. 2014, The Astrophysical Journal, 796, 132

Dumusque, X., Udry, S., Lovis, C., Santos, N. C., & Monteiro, M. J. P. F. G. 2011, A&A, 525, A140

Dumusque, X., Glenday, A., Phillips, D. F., et al. 2015, The Astrophysical Journal Letters, 814, L21

Fischer, D. A., Anglada-Escude, G., Arriagada, P., et al. 2016, Publications of the Astronomical Society of the Pacific, 128, 066001

Giorgini, J. D., Yeomans, D. K., Chamberlin, A. B., et al. 1996, in Bulletin of the American Astronomical Society, Vol. 28, AAS/Division for Planetary Sciences Meeting Abstracts #28, 1158

Gray, D. 2005, The Observation and Analysis of Stellar Photospheres (Cambridge University Press)

Gray, D. F. 2009, The Astrophysical Journal, 697, 1032

Gray, D. F., & Oostra, B. 2018, The Astrophysical Journal, 852, 42

Haywood, R. D., Collier Cameron, A., Unruh, Y. C., et al. 2016, Monthly Notices of the Royal Astronomical Society, 457, 3637

Howell, S. B., Sobeck, C., Haas, M., et al. 2014, Publications of the Astronomical Society of the Pacific, 126, 398

Isaacson, H., & Fischer, D. 2010, ApJ, 725, 875

Kurucz, R. L. 2005, http://kurucz.harvard.edu/sun/fluxatlas2005/

Kurucz, R. L., Furenlid, I., Brault, J., & Testerman, L. 1984, Solar flux atlas from 296 to 1300 nm (National Solar Observatory)

Mayor, M., & Queloz, D. 1995, Nature, 378, 335

Meunier, N. 2018, A&A, 615, A87

Meunier, N., Desort, M., & Lagrange, A.-M. 2010a, A&A, 512, A39

Meunier, N., & Lagrange, A.-M. 2019, A&A, 625, L6

Meunier, N., Lagrange, A.-M., Borgniet, S., & Rieutord, M. 2015, A&A, 583, A118

Meunier, N., Lagrange, A.-M., & Desort, M. 2010b, Astronomy and Astrophysics, 519, A66

Meunier, N., Lagrange, A.-M., & Borgniet, S. 2017a, A&A, 607, A6

Meunier, N., Lagrange, A.-M., Mbemba Kabuiku, L., et al. 2017b, A&A, 597, A52

Milbourne, T. W., Haywood, R. D., Phillips, D. F., et al. 2019, The Astrophysical Journal, 874, 107

Motalebi, F., Udry, S., Gillon, M., et al. 2015, A&A, 584, A72

Norton, A. A., Graham, J. P., Ulrich, R. K., et al. 2006, Solar Physics, 239, 69

Palle, P. L., Jimenez, A., Perez Hernandez, F., et al. 1995, ApJ, 441, 952

Pepe, F. A., Cristiani, S., Lopez, R. R., et al. 2010, Proc.SPIE, 7735, 7735

Phillips, D. F., Glenday, A. G., Dumusque, X., et al. 2016, Proc. SPIE, Advances in Optical and Mechanical Technologies for Telescopes and Instrumentation II

Reiners, A., Mrotzek, N., Lemke, U., Hinrichs, J., & Reinsch, K. 2016, A&A, 587, A65

Ricker, G. R., Winn, J. N., Vanderspek, R., et al. 2014, Journal of Astronomical Telescopes, Instruments, and Systems, 1, 1

Saar, S. H., & Donahue, R. A. 1997, The Astrophysical Journal, 485, 319

Schrijver, C. J., & Zwaan, C. 2000, Solar and Stellar Magnetic Activity, Cambridge Astrophysics (Cambridge University Press)

Schroeter, E. H. 1984, A&A, 139, 538

Shelke, R. N., & Verma, V. K. 1985, Bulletin of the Astronomical Society of India, 13, 53

Sosnowska, D., Lodi, M., Gao, X., et al. 2012, Proc.SPIE, 8451, 8451

VanderPlas, J., Connolly, A. J., Ivezić, Ž., & Gray, A. 2012, in 2012 Conference on Intelligent Data Understanding, 47

VanderPlas, J. T., & Ivezić, Ž. 2015, The Astrophysical Journal, 812, 18

Zechmeister, M., & Kürster, M. 2009, A&A, 496, 577